JOURNAL OF SYNCHROTRON RADIATION

ISSN 1600-5775

Performance on absolute scattering intensity calibration and protein molecular weight determination at BL16B1, a dedicated SAXS beamline at SSRF

Jianrong Zeng, Fenggang Bian,* Jie Wang,* Xiuhong Li, Yuzhu Wang, Feng Tian and Ping Zhou

Shanghai Institute of Applied Physics, Chinese Academy of Sciences, Zhangheng Road 239, Pudong District, Shanghai 201204, People's Republic of China.
*Correspondence e-mail: bianfenggang@sinap.ac.cn, wangjie@sinap.ac.cn

Received 28 June 2016
Accepted 1 December 2016

Edited by M. Yabashi, RIKEN SPring-8 Center, Japan

Keywords: beamline; SAXS; absolute intensity; calibration; molecular weight.

The optical system and end-station of bending-magnet beamline BL16B1, dedicated to small-angle X-ray scattering (SAXS) at the Shanghai Synchrotron Radiation Facility, is described. Constructed in 2009 and upgraded in 2013, this beamline has been open to users since May 2009 and supports methodologies including SAXS, wide-angle X-ray scattering (WAXS), simultaneous SAXS/WAXS, grazing-incidence small-angle X-ray scattering (GISAXS) and anomalous small-angle X-ray scattering (ASAXS). Considering that an increasing necessity for absolute calibration of SAXS intensity has been recognized in in-depth investigations, SAXS intensity is re-stated according to the extent of data processing, and the absolute intensity is suggested to be a unified presentation of SAXS data in this article. Theory with a practical procedure for absolute intensity calibration is established based on BL16B1, using glass carbon and water as primary and secondary standards, respectively. The calibration procedure can be completed in minutes and shows good reliability under different conditions. An empirical line of scale factor estimation is also established for any specific SAXS setup at the beamline. Beamline performance on molecular weight (MW) determination is provided as a straightforward application and verification of the absolute intensity calibration. Results show good accuracy with a deviation of less than 10% compared with the known value, which is also the best attainable accuracy in recent studies using SAXS to measure protein MW. Fast MW measurement following the demonstrated method also enables an instant check or pre-diagnosis of the SAXS performance to improve the data acquisition.

1. Introduction

Two phenomena, absorption and scattering, occur when X-rays interact with matter. Small-angle X-ray scattering (SAXS) refers to the scattering phenomenon near the incident beam, typically with a small scattering angle of less than 10° (Schnablegger, 2011; Svergun & Koch, 2003; Zhu, 2008). The advent of synchrotron X-ray sources offered new possibilities in SAXS in addition to delivering enhanced photon flux; for instance, small source size and low divergence, and tenability of photon energy (Narayanan, 2008). Using synchrotron radiation X-ray sources, SAXS can be an *in situ* and nondestructive way to characterize the heterogeneity of a characteristic length usually within 1–100 nm and has been widely used in analyses of soft matter such as fibres, polymers, colloids, liquid crystals, proteins and other biological macromolecules. It is a steadily advanced tool for structural char-

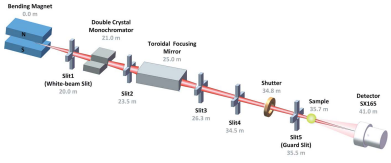

acterization on the nano-scale and has an impact on diverse fields of study (Li *et al.*, 2016; Narayanan, 2008). Over decades, quite a number of beamlines dedicated to SAXS based on the third-generation synchrotron facilities, such as 12-ID and 15-ID at the Advance Photon Source (APS) in USA, ID02 at the European Synchrotron Radiation Facility (ESRF) in France, I22 at the Diamond Light Source in the UK, SAXS/WAXS beamline at the Australian Synchrotron in Australia, 40B2 at SPring-8 in Japan and 4C at the Pohang Accelerator Laboratory (PAL) in Korea *etc.*, have been developed worldwide. A bending-magnet beamline, BL16B1, for SAXS was constructed as one of the seven Phase-I beamlines at Shanghai Synchrotron Radiation Facility (SSRF), the first third-generation synchrotron radiation light source in mainland China (Xu & Zhao, 2008; Cyranoski, 2009). Opened to users in 2009 and upgraded in 2013, beamline BL16B1 provides various scattering-related techniques in nano-scale structure characterization and enables time-resolved studies on structural transitions at the sub-second level. A series of ancillary facilities are also available for *in situ* experiments. Since the opening, it has played an important role in supporting studies from a queue of scientists waiting for beam time, and over 350 (October 2016) users' publications have been attributed to this beamline.

Quality data acquisition and processing are key procedures in structural characterization using SAXS. The raw data measured in a SAXS experiment are not usually adequate for any quantitative conclusion to be made concerning the issues under investigation. The one-dimensional (1D) raw intensity data, including that converted from the original two-dimensional (2D) detected graphs, usually have the form of counts or arbitrary units (a.u.) (typically in counts per second). They can be used to observe the scattering orientation and judge the phase transition peak. If the raw intensity is converted into a normalized form, it can further be used to calculate the radius of gyration and the correlation function. It also can be used to fit the form and structure factors in some restricted models. Once the intensity is calibrated onto the absolute scale, it can be further used to calculate or determine the molecular weight of the sample material, the density of the scattering length of phases in multiphase systems, the number density of the scattering particles, the volume fraction and the specific surface (Fan *et al.*, 2010). It also can be used to detect artifacts in SAXS data and restrict the fitting parameters for a given model to match the observed intensities (Zhang *et al.*, 2009). Moreover, as the absolute intensity is independent of the experimental settings or parameters such as the intensity of the incident beam, exposure time and sample thickness, it can be used to compare or unify measurements of the same material between various settings or instruments, and to stitch SAXS and WAXS (wide-angle X-ray scattering) data (Fan *et al.*, 2010). Thus, absolute intensity calibration is important for subsequent data analysis and experimental methodology development in SAXS. However, not many works can be found dealing with these topics and few practical calibration procedures have been acknowledged in SAXS performance among various devices.

One of the most straightforward applications of SAXS is the determination of molecular weight (MW) in the characterization of macromolecules (Fischer *et al.*, 2010). It is also very useful in determinating the oligomeric state of biomolecules and monitoring aggregation or degradation processes (Mylonas & Svergun, 2007). Although it is less accurate compared with using mass spectroscopy, MW determination using SAXS can be an *in situ* method which allows biomolecule samples in solution, closer to their native state. In the SAXS performance, one can assess the protein MW using the relative intensity or the absolute intensity separately. Existing research is mainly focused on the former method as the intensity is not always calibrated onto the absolute scale. However, using the relative intensity usually requires measuring additional SAXS curves of standard protein of known value for comparison (Mylonas & Svergun, 2007). Moreover, suitable uniform standard protein can hardly be determined as protein MW varies from tens of kDa (1 kDa = 1000 g mol^{-1}) to hundreds of kDa. A couple of ways of using the relative intensity have also been proposed to assess the protein MW without measuring additional standard protein (Pleštil *et al.*, 1991; Fischer *et al.*, 2010). However, these methods depend highly on the scattering range, and uncertainty in the experimental scattering curves or an improper choice of the integration limit can lead to erroneous results. On the contrary, once the intensity is calibrated onto the absolute scale one can directly determine the protein MW with less uncertainty and without measuring any standard protein materials. Experimental protein MW in agreement with the expected value also can provide confidence that the sample contains monodisperse particles of the expected composition, and analysis of the data to extract structural parameters can further proceed (Jacques *et al.*, 2012).

In the following sections, the photon source and optical arrangement of the SAXS beamline BL16B1 at SSRF are briefly described. The experimental hutch and installed equipment for different configurations are also introduced. Theory for absolute scattering intensity calibration using both primary and secondary standard is established based on this beamline. The repeatability and reliability performance of the calibration procedure were also tested using different setups. The MW of several proteins frequently used in the laboratory are determined using the calibrated absolute intensity as an application and verification of the calibration. Guidance for sample preparation as well as experiment operation and prediagnosis on data quality suggested by the quick MW determination are also discussed. This paper presents a dedicated SAXS beamline with performance to make meaningful immediate improvement in the acquirement and processing of quality data for in-depth analysis during the experiments.

2. Beamline overview

Fig. 1 shows the general beamline and optical layout. The beamline was designed using a 1.27 T bending-magnet photon source delivering intense radiation, from which the beam with a divergence of 1.2 mrad (H) × 0.12 mrad (V) can be accepted

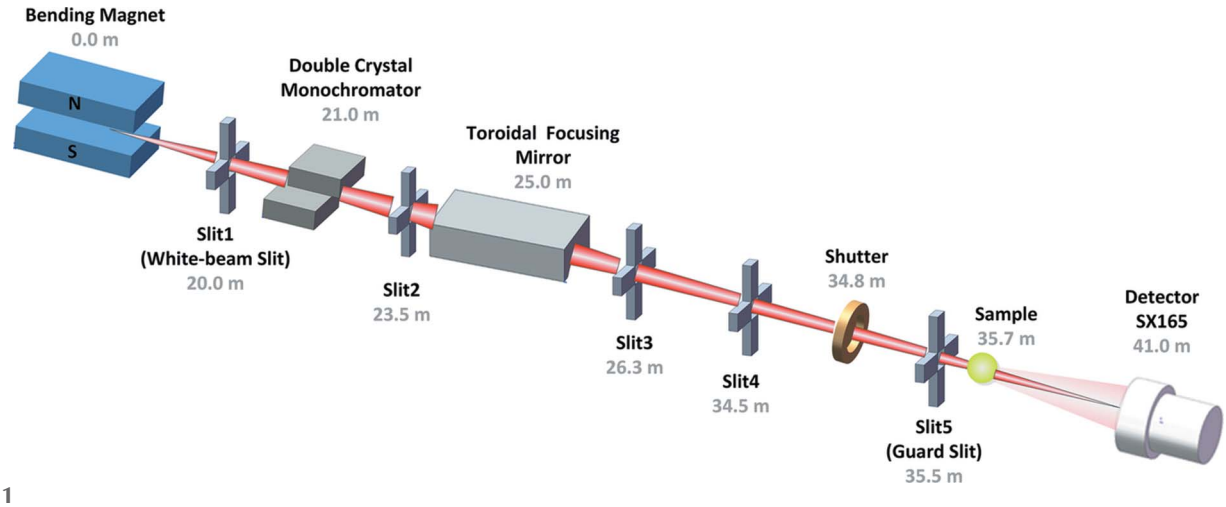

Figure 1
Optical scheme of beamline BL16B1 with bending-magnet X-ray source, Si(111) DCM, toroidal focusing mirror and collimating slits. The focus spot is at 41.0 m from the source. The end-station, where sample and detector are indicated, is described in detail in §2.2.

by the optics system. A flat Si(111) double-crystal monochromator (DCM) is used for X-ray monochromatization within 5–20 keV and a double-focusing toroidal mirror is used to focus the beam size to 0.4 mm (H) × 0.5 mm (V) at the detecting plane. The SSRF storage ring operates at 3.5 GeV with a typical top-up current around 250 mA (October 2016). A collimated flux of $\sim 10^{12}$ mm^2 s^{-1} at 10 keV can be regularly introduced for the SAXS performance at the beamline end-station. Table 1 lists the characteristics of the beamline.

Table 1
Specifications of beamline BL16B1.

Parameters	Specifications
Source	Bending magnet
Monochromator	Si(111) DCM
Energy range (keV)	5–20
Energy resolution ($\Delta E/E$ @ 10 keV)	4.0×10^{-4}
Flux (photons s^{-1} @ 10 keV and 240 mA)	$\sim 3 \times 10^{11}$
Focus size (H × V) (mm)	0.4 × 0.5
Divergence (H × V) (mrad)	1.8 × 0.16

2.1. End-station and methodologies

The layout of the beamline end-station is shown schematically in Fig. 2. To reduce air scattering, the incident X-ray beam is introduced within vacuum tubes with a gap for placing the sample stage. The lengths of both upstream and downstream tubes are adjustable, which allows the sample-to-detector distance L (m) to be variable. An ion chamber inserted in the vacuum tube and a photodiode mounted on the beamstop are used as the upstream detector and downstream detector for beam intensity monitoring before and after the sample, respectively. The SAXS data are collected using a Rayonix SX165 detector with a diameter of 165 mm and 2048 × 2048 pixels. Considering the beamstop has a diameter of 6 mm and L is regularly set at 2 and 5 m, the typical q (nm^{-1}) range detected for SAXS is within 0.06–3.50 nm^{-1}. Here $q = 4\pi \sin\theta/\lambda$ is the modulus of the scattering vector $\mathbf{q}$ where 2θ (°) is the scattering angle and λ (nm) is the X-ray wavelength. WAXS, with a typical q range over 2.50 nm^{-1}, can be performed by placing the sample stage between the downstream tubes and the SX165 detector.

Besides SAXS and WAXS, methodologies such as 2D simultaneous SAXS/WAXS, grazing-incident small-angle X-ray scattering (GISAXS) and anomalous small-angle X-ray scattering (ASAXS) can also be performed in different

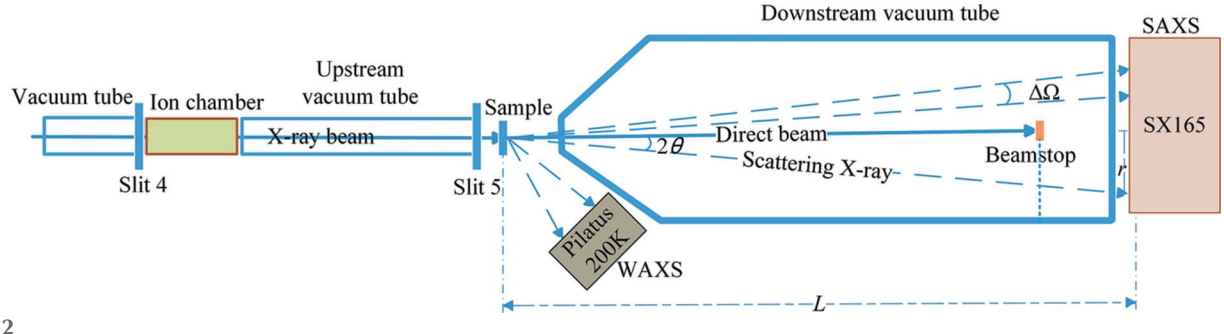

Figure 2
Schematic layout of the instrumentation in the end-station at beamline BL16B1. The SX165 detector can be used both for SAXS and WAXS detection by placing the sample before and after the downstream tube, respectively. The Pilatus 200K detector can also be used for WAXS but more frequently for simultaneous 2D SAXS/WAXS measurement. 2θ is the scattering angle, $\Delta\Omega$ is the unit solid angle centered on an arbitrary scattering direction associated with $\mathbf{q}$, L is the distance between the sample and detector and r is the distance from the pixel to the direct beam center.

configurations at this beamline. To achieve simultaneous SAXS/WAXS, a Pilatus 200K detector is set aside the beam path for detecting WAXS. This detector, mounted on an adjustable stage, can be placed near the sample quite flexibly such that an adjustable WAXS q range (typically 2.50–34.8 nm^{-1}) is available. For GISAXS measurement, a Kohzu tilt stage is used as the sample stage and the incidence angle of X-rays can be adjusted with an accuracy of 0.001° in a range of ±10° (Tian *et al.* 2015). Special GISAXS on liquid surfaces can also be performed as the incident beam has a downward inclination of 6.4 mrad after passing through the focusing mirror. Energy tunability of the DCM makes ASAXS conduction achievable and ASAXS of Al–Zn alloys has been carried out recently (Yang *et al.*, 2016). Grazing-incident wide-angle X-ray scattering (GIWAXS) is also developing and should be open to users very soon.

2.2. Sample environment and ancillary facilities

A series of commercial and customized *in situ* devices are available, including a Linkam THMS600 heating stage (−196°C to 600°C), a Linkam CSS450 shearing system (from room temperature to 450°C), a Linkam TS1500 heating stage (up to 1500°C), an *in situ* fiber stretching and heating device (maximum tension of 1000 N and up to 500°C), a microfluidic peristaltic device and a helium-atmosphere sample chamber to protect the samples from oxidation. More devices such as a GISAXS heating chamber and relative humidity controlling chamber are also being produced. Besides the foreseen sample surroundings, the beamline also reserves the ability to install the users' own specialized sample devices, as has happened in a series of works (Zhou *et al.*, 2015; Liu *et al.*, 2014; Li *et al.*, 2014; Huang *et al.*, 2014). Supporting laboratories with ultra-pure water system, magnetic stirrer, electronic balance, ultrasonic apparatus, centrifuge, electric oven, vacuum drying apparatus, polarizing microscope and atomic force microscope are also provided for users.

2.3. Experiment control and data analysis

The beamline control system, including both the optical system and the experimental controlling devices, is built based on an EPICS platform using the Linux operation system, which is convenient for communicating among the devices. The experimental control panel includes several most frequently used experimental modes such as normal SAXS/WAXS, heating SAXS/WAXS, simultaneous SAXS/WAXS and GISAXS. Special modules can also be added when users' customized devices are installed for the experiments. Widely used packages for SAXS/WAXS/GISAXS data processing such as *FIT2D*, *Nika*, *Irena* and *X-polar* have been installed for users. Special data process services such as remote data access and data archive are also available on request (Hu *et al.*, 2014).

3. Beamline performance on absolute scattering intensity calibration

3.1. General theory for absolute intensity calibration

3.1.1. Intensity description. When dealing with radiation phenomena, flux (j) is the original quantity used to describe the strength of a beam of radiation. However, it is well known that in SAXS the scattering flux j_{sc} will increase or decrease in proportion to the incident flux j_{in} such that the ratio j_{sc}/j_{in} as a function of the scattering direction, which is related to the structure of the scatterer, is what we are really interested in. This ratio is invariably referred to as the differential scattering cross section (Roe, 2000) and is also exactly what the so-called scattering intensity stands for in general discussion,

$$I(q) = \frac{d\sigma}{d\Omega} \equiv \frac{j_{sc}}{j_{in}}, \tag{1}$$

in which $I(q)$ is typically in $cm^2\ sr^{-1}$ as a function of q (nm^{-1}) and $q = 4\pi \sin\theta/\lambda$ is the modulus of the scattering vector $\mathbf{q}$ where 2θ (°) is the scattering angle and λ (nm) is the X-ray wavelength. j_{in} ($cm^{-2}\ s^{-1}$) is measured as the amount of particles (such as photons or neutrons) transmitted per unit area per second as the incident beam is usually a plane wave, while j_{sc} ($sr^{-1}\ s^{-1}$) is expressed as the amount of particles transmitted per second through a unit solid angle rather than a unit area for the scattering spherical wave. j_{in} and j_{sc} can be written as

$$j_{in} = \frac{dN_{in}}{dA\,dt}, \tag{2a}$$

$$j_{sc} = \frac{dN_{sc}}{d\Omega\,dt} = R^2 \frac{dN_{sc}}{dS\,dt}, \tag{2b}$$

where N_{in} (counts) is the number of incident particles and N_{sc} (counts) is the number of scattering particles, A (cm^2) is the cross-section area of the incident beam, Ω (sr) is the solid angle centered on a particular scattering direction associated with $\mathbf{q}$, R (m) is the distance from the scattering source to the point of observation, S (cm^2) is the detecting area on the scattering spherical surface with radius R, and t (s) is the exposure time.

In actual SAXS experiments, the detected scattering raw intensity $C(q)$ (counts) is a particle number read out by the detector. It is not exactly equal to the particles scattered from the sample $N_{sc}(q)$. On one hand, $N_{sc}(q)$ can be partly absorbed by the sample itself and the surrounding air during the propagation to the detector; on the other hand, besides $N_{sc}(q)$, scattering from the background related to the instrumentation (mainly from the sample holder and the surrounding air), noted as $C_{bg}(q)$, can also be read out by the detector. Considering the detector efficiency $\eta(\lambda)$ and the (X-ray) transmission coefficient $T(\lambda)$, $C(q)$ should be (Fan *et al.*, 2010; Narayanan, 2008)

$$\begin{aligned} C(q) &= \eta(\lambda)\,T(\lambda)\,N_{sc}(q) + C_{bg}(q) \\ &= \eta(\lambda)\,T(\lambda)\,j_{in}\,\Delta\Omega t\,I(q) + C_{bg}(q), \end{aligned} \tag{3}$$

and

$$I(q) = \frac{[C(q) - C_{bg}(q)]}{\eta(\lambda)\, T(\lambda)\, j_{in}\, \Delta\Omega t} = \frac{1}{\eta(\lambda)\, j_{in}\, \Delta\Omega} \frac{[C(q) - C_{bg}(q)]}{T(\lambda)\, t} = \mathrm{GF}\, I_n(q), \quad (4)$$

where GF (cm^2 s sr^{-1}) is the general intensity scale factor and $I_n(q)$ (s^{-1} or a.u.) is the normalized intensity for general intensity,

$$\mathrm{GF} = \frac{1}{\eta(\lambda)\, j_{in}\, \Delta\Omega}, \quad (5)$$

$$I_n(q) = \frac{[C(q) - C_{bg}(q)]}{T(\lambda)\, t}. \quad (6)$$

It worth noting that the scope of $\Delta\Omega$ usually depends on the detector, typically restricted to the area of a pixel ΔS. It is easy to see that GF is only related to the experimental setup and is independent of the sample as long as the sample is sufficiently large (*i.e.* larger than the incident beam). Once the experimental conditions are set, GF can be regarded as a constant, enabling one to use $I_n(q)$ instead of $I(q)$ in general discussion. This is quite meaningful as the determination of GF is a time-consuming and laborious work but shows no specific necessity.

The absolute intensity I_{abs} (q) (cm^{-1} sr^{-1}), also noted as $d\Sigma/d\Omega$, is defined as the differential scattering cross section per unit sample volume V (cm^3) (Orthaber *et al.*, 2000; Roe, 2000; Zhang *et al.*, 2009; Fan *et al.*, 2010),

$$I_{abs}(q) = \frac{d\Sigma}{d\Omega} = \frac{1}{V}\frac{d\sigma}{d\Omega}. \quad (7)$$

It is the physical quantity used to quantify the scattering ability of a specific material to the X-rays. It is also an intensive property of the specific material and not dependent on the physical dimensions or amount of the sample. $I_{abs}(q)$ can be written as

$$I_{abs}(q) = \frac{I(q)}{V} = \frac{\mathrm{GF}\, I_n(q)}{Al} = \mathrm{SF}\, I_n(q)/l, \quad (8)$$

$$\mathrm{SF} = \frac{\mathrm{GF}}{A} = \frac{1}{\eta(\lambda)\, j_{in}\, A\, \Delta\Omega} = \frac{1}{\eta(\lambda)\, J_{in}\, \Delta\Omega}, \quad (9)$$

where $V = Al$ and l (cm) is the sample thickness, SF (s sr^{-1}) is the absolute intensity scale factor, and $J_{in} = j_{in}A$ is the total incident flux (s^{-1}) illuminated on the sample. It is easy to see that SF is only a matter of the experimental setup and, once calculated, can be used to turn the normalized intensity into absolute scale.

It is necessary to distinguish the raw intensity $C(q)$, general intensity $I(q)$ and absolute intensity $I_{abs}(q)$ in SAXS data analyses. A misapplication of $C(q)$ or $I(q)$ can give a result that is not really what it appears. Table 2 summarizes the common circumstances of SAXS analysis in which these three intensities should be used and what can be done using them. Although the general intensity $I(q)$ can be obtained much more easily and seems sufficient to meet the needs of use in quite a lot of situations including some model fitting, $I_{abs}(q)$ can be used to do much more comprehensive work. $I_{abs}(q)$ can also be chosen as the unified presentation of SAXS data on the condition that it is available in experiments. As a matter of fact, instead of $I(q)$, $I_{abs}(q)$ is becoming the priority choice in general discussion and also preferred in in-depth data analyses in recent years (Li *et al.*, 2016; Narayanan, 2008; Ilavsky & Jemian, 2009; Svergun & Koch, 2003). In particular, $I_{abs}(q)$ is required to evaluate molar masses of suspended particles in a direct way from the SAXS curve.

Table 2
Common circumstances of SAXS analysis in which $C(q)$, $I(q)$ and $I_{abs}(q)$ should be used.

Circumstance	$C(q)$ (counts)	$I(q)$ (cm^2 sr^{-1}) or $I_n(q)$ (s^{-1})	$I_{abs}(q)$ (cm^{-1} sr^{-1})
Observing scattering orientation	Yes	Yes	Yes
Judging phase transition peak	Yes	Yes	Yes
Calculating radius of gyration	No	Yes	Yes
Correlation functions derivation	No	Yes	Yes
Form factor and structure factor fitting in restricted model	No	Yes	Yes
Molecular weight determination	No	No†	Yes
Quantifying the invariant	No	No	Yes
Calculating scattering length density in multiphase systems	No	No	Yes
Calculating volume fraction and specific surface area of particles	No	No	Yes
Restricting fitting parameters for given model	No	No	Yes
Artifacts detecting	No	No	Yes
Subtraction of incoherent part to obtain the coherent component	No	No	Yes

† The molecular weight of proteins can be determined using $I(q)$ in quite an indirect way but improper choice of the integration limit might lead to erroneous results (Pleštil *et al.*, 1991; Fischer *et al.*, 2010).

3.1.2. Calibration. Theoretically, $I_{abs}(q)$ can be calculated by measuring the parameters in equations (8) and (9) one by one; this is called primary calibration. In practice, the intensity of the incident beam is generally much larger than the scattering intensity, especially when using a synchrotron radiation X-ray source. Most of the time, the incident intensity and scattering intensity measurements require different types of detectors. Owing to different detecting principles and detecting efficiencies, this often results in the two measurements being hardly comparable. Therefore, $I_{abs}(q)$ is barely measured in the direct way. Instead, a sample with known $I_{abs}(q)$ is usually used as a standard while the correction factor or scale factor SF for an actual setup can be obtained by measuring this standard and comparing with the known value. The scattering intensity of other samples detected in the same setup then can be corrected to the absolute scale using this SF; this is called secondary calibration. According to equation (9), the quantities determined by the instrument settings such as J_{in}, $\Delta\Omega$ and $\eta(\lambda)$ can be separated to form the scale factor. The quantities related to the sample such as $T(\lambda)$, l, t and $I_{bg}(q)$ can be regarded as the corrections or normalization of $I(q)$ and further form $I_n(q)/l$.

The normalized scattering intensity of the standard $I_{n,st}(q)$ can be directly measured, and SF can be calculated as

$$\mathrm{SF} = I_{\mathrm{abs,st}}(q)\, l_{\mathrm{st}}/I_{\mathrm{n,st}}(q), \tag{10}$$

where $I_{\mathrm{abs,st}}(q)$ is the known absolute scattering intensity of the standard. Considering that 2θ is very small such that $\Delta\Omega$ associated with different $\mathbf{q}$ can be treated as a constant in the same setup, then SF does not vary theoretically with q. A value calculated at a single q or a mean value calculated over various q can be used for SF. Once SF was calculated, $I_{\mathrm{abs}}(q)$ of a sample detected in the same setup can be calculated using equation (8).

The standards used in SAXS absolute intensity calibration can be divided into two categories. One is that the absolute intensity of the standard itself is obtained using the primary calibration method, called the primary standard. The other is that the absolute intensity of the standard itself is obtained or calibrated by using the primary standard; such a standard is referred to as the secondary or indirect standard. Glassy carbon is a strong scatterer and has such stable thermal properties that it can be used as a well investigated primary standard. However, as an *ad hoc* standard, calibrated glassy carbon samples are still being made available to research laboratories and facilities around the world in order to facilitate in-depth SAXS analysis (Zhang *et al.*, 2009). Other potential primary standards such as polyethylene (Lupolen) and SiO_2 particles in elastomer also have encountered quite a lot of difficulties in manufacturing or distributing the well calibrated samples. Scattering from a single-component liquid or gas originates from the thermal density fluctuation and shows an angle-independent profile (Roe, 2000; Orthaber *et al.*, 2000; Narayanan, 2008), making some specific pure liquid be an appropriate secondary standard. Although pure water has a very weak scattering that varies with temperature, it can be obtained and handled very easily experimentally. What is more, water is also a ubiquitous solvent for solution samples that it can potentially be a practical secondary standard, especially for bio-samples. However, few reported data can be found using water as calibration reference. A probable reason is that water scattering measurement is quite time-consuming, especially for conventional X-ray sources. Nowadays, high-brilliance synchrotron radiation X-ray sources are becoming much more available and the use of water as a practical reference for fast calibration can be re-evaluated. The scattering of pure water at the limit $q \rightarrow 0$ only depends on the physical property of isothermal compressibility, that is (Fan *et al.*, 2010; Roe, 2000; Weinberg, 1963)

$$I_{\mathrm{abs,water}}(0) = \rho_{\mathrm{water}}^2 k\tau\beta, \tag{11}$$

where ρ_{water} (cm^{-2}) is the scattering length density of water, k ($= 1.381 \times 10^{10}\ \mathrm{J\ K^{-1}}$) is the Boltzmann constant, τ is the temperature and β is the isothermal compressibility. At room temperature ($\tau = 298$ K), the density d of water is $0.9970\ \mathrm{g\ cm^{-3}}$, $\rho_{\mathrm{water}} = 9.403 \times 10^{10}\ \mathrm{cm^{-2}}$, $\beta = 4.524 \times 10^{-10}\ \mathrm{Pa^{-1}}$ (Lide, 2005) and $I_{\mathrm{abs,water}}(0) = 1.646 \times 10^{-2}\ \mathrm{cm^{-1}\ sr^{-1}}$. SF can be calculated using this unique value as $\mathrm{SF} = I_{\mathrm{abs,water}}(0)\, l_{\mathrm{water}}/I_{\mathrm{n,water}}(0)$.

3.1.3. Reduction and normalization of raw intensity. More detailed theory for SAXS data reduction and correction can be found in published works (Pauw, 2013; Narayanan, 2008; Fan *et al.*, 2010). Several key issues involving absolute intensity calibration should be considered in actual experiments. As expressed in equation (6), detected intensity normalization includes background subtraction and correction against exposure time and transmission coefficients. In an actual measurement, two additional factors can contribute to the detected counts even without the presence of an X-ray beam. One is caused by the detector electronics settings such as the pedestal bias, and the other is from the omnipresent natural radiation. They can be simultaneously considered as the so-called 'dark current'. Generally, the dark current $C_{\mathrm{dc}}(t)$ includes a time-independent component, a time-dependent component and a flux-dependent component. However, the time-independent component would be the base amount for detectors based on photomultiplier tubes and charge coupled devices (CCDs). It is homogeneously distributed over the entire detector and can be corrected by subtraction of a single value from each detected pixel value (Pauw, 2013). Fig. 3 shows the total counts in different integrated time measured by the Rayonix SX165, a type of CCD detector, used in this work. It can be seen that the dark current is horizontal along the q axis (*i.e.* detector pixels) and nearly independent of time.

For most samples with strong scattering intensity, $C_{\mathrm{dc}}(t)$ shows few effects on $I_{\mathrm{n}}(q)$. But for samples with very weak scattering such as pure water, $C_{\mathrm{dc}}(t)$ will obviously affect the detected signal. Including the deduction of $C_{\mathrm{dc}}(t)$ and considering that $C(q)$ and $C_{\mathrm{bg}}(q)$ are obtained in virtually two separate single measurements, the normalization should be further written as

$$I_n(q) = \frac{[C(q) - C_{\mathrm{dc}}(t)]/t}{T(\lambda)} - \frac{[C_{\mathrm{bg}}(q) - C_{\mathrm{dc}}(t)]/t_{\mathrm{bg}}}{T_{\mathrm{bg}}(\lambda)}, \tag{12}$$

where t_{bg} is the exposure time of $C_{\mathrm{bg}}(q)$.

Regarding SAXS performance, the samples are always placed on/in some sample holder, usually in air in order to facilitate replacement of the samples. This will inevitably bring

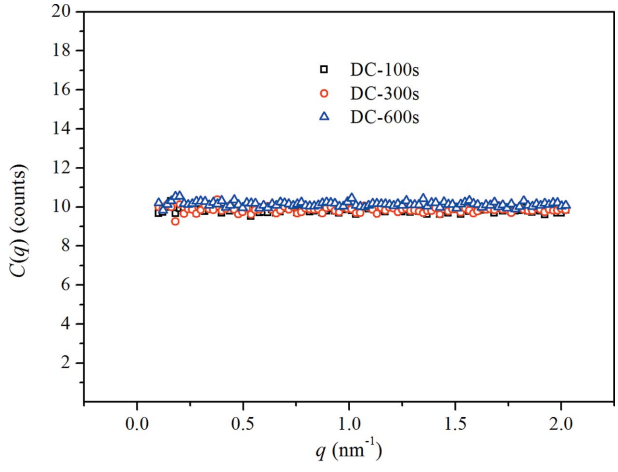

Figure 3
The dark current of SX165. DC-100s, DC-300s and DC-600s were detected with an exposure time of 100 s, 300 s and 600 s, respectively.

about background scattering. For a solid sample, $C_{bg}(q)$ refers to air scattering along the direct incident beam route. For a liquid sample, as the liquid is always placed in the holder (*e.g.* a cell or capillary), $C_{bg}(q)$ refers to scattering from the empty holder and the air along the direct incident beam. The sample absorption, *i.e.* $T(\lambda)$, can be calculated by measuring the intensity of the incident beam before and after it passes through the sample. Assuming a linear response for both upstream and downstream detectors, if the quantum efficiency is the same, $T(\lambda)$ is equal to i_{down}/i_{up}, where i_{down} and i_{up} are readings of the upstream and downstream detectors, respectively. However, the upstream and downstream detectors are usually of different types (*e.g.* ion chamber and pin-diode) and have different quantum efficiencies most of the time. In this condition, $T(\lambda)$ should be scaled by the quantum efficiency difference factor,

$$T(\lambda) = \frac{(i_{down}/i_{up})_{sample}}{(i_{down}/i_{up})_{air}}, \quad (13)$$

where the subscripts 'sample' and 'air' denote the condition with and without the sample inserted in the beam route, respectively. Here, note that 'without sample' does not mean there is nothing in the beam route as air still remains. For the background absorption $T_{bg}(\lambda)$, one can treat the object causing the background scattering as the 'sample' inserted in the beam route and use equation (13) to perform the same calculation. This means that, for a liquid sample in the holder, $T_{bg}(\lambda)$ can be calculated as

$$T_{holder}(\lambda) = \frac{(i_{up}/i_{down})_{holder}}{(i_{up}/i_{down})_{air}}, \quad (14)$$

where 'holder' denotes the condition with the empty holder inserted as the sample in the beam route. For a solid sample directly exposed to the beam, $T_{bg}(\lambda) = 1$. This means that the background (*i.e.* air) scattering is not absorbed by any insertion object in the beam route. The sample thickness l can be measured using a tool such as venire calipers or can be calculated using the transmission coefficient as follows,

$$T(\lambda) = \exp(-\mu_m dl), \quad (15)$$

$$l = \frac{\ln T(\lambda)}{-\mu_m d}. \quad (16)$$

For water, when the incident photon energy is 10 keV, μ_m = 5.329 cm^2 g.

3.2. Calibration performance

The photon energy of the X-ray was set at 10 keV and the room temperature was kept at 25°C for the calibration experiments. Groups of settings were used in the experiments by varying the beam flux and the distance between the sample and the detector. Glass carbon and pure water with a resistivity of 18 MΩ cm^{-1} were used as first and second standard, respectively, to calibrate the absolute scattering intensity. The standard glass carbon and its absolute scattering intensity profile was provided by 15ID at APS.

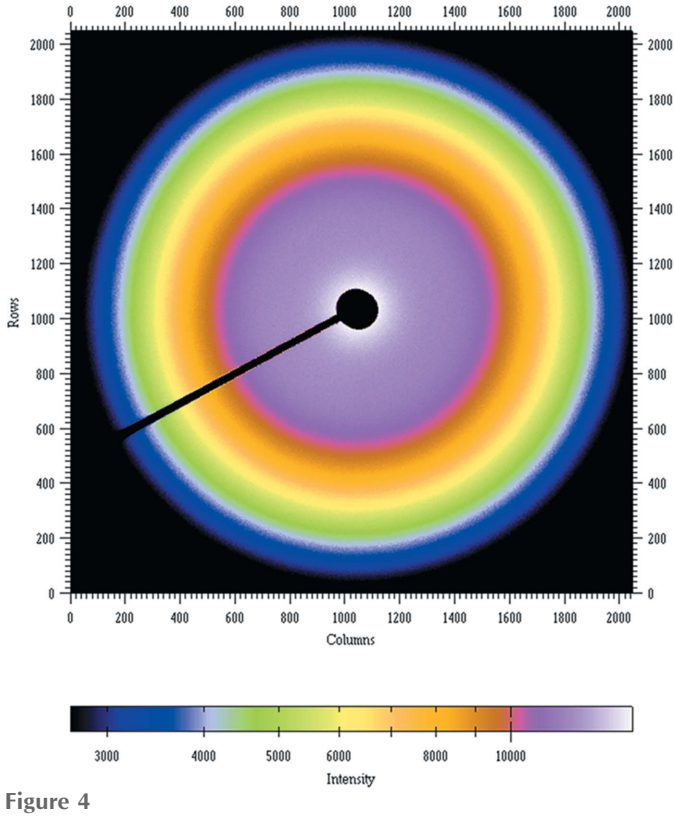

Figure 4
2D scattering graph of glass carbon read out by the SX165 detector.

3.2.1. Calibration using glass carbon as first standard. Fig. 4 shows the measured 2D scattering intensity distribution of glass carbon. Deducting the background scattering from air and normalizing according to equation (12), the 1D intensity of glass carbon was transformed into a scale of cm^2 s^{-1} (Fig. 5). The calibrated data measured here showed good coincidence with the referenced data (Fig. 6). Compared with the 1D absolute scattering intensity measured at beamline 15ID of APS using the direct method, the SF for the setup here can be calculated to be 0.0185 s sr^{-1} using equation (10). The normalized scattering profiles were completely reproduced

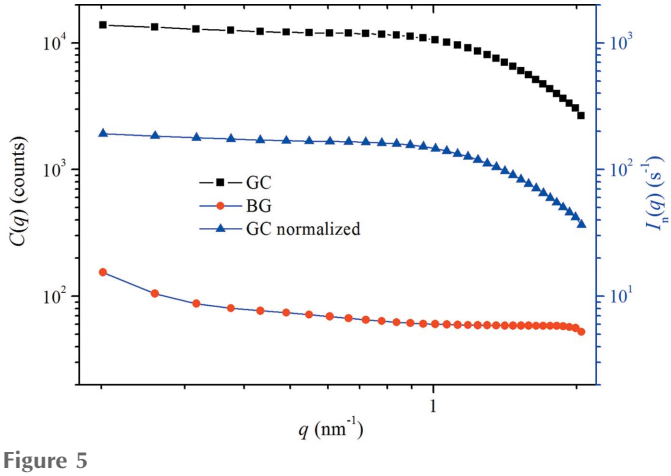

Figure 5
Scattering profile of glass carbon: raw intensity and normalized. The exposure time is 100 s for both the glass carbon (GC) and the background (BG).

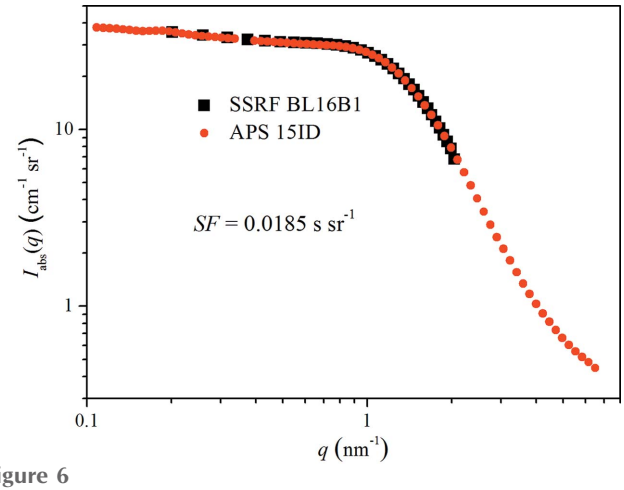

Figure 6
1D scattering intensity of glass carbon. By comparison with the calibrated intensity, SF = 0.0185 s sr^{-1}.

and the SF value remained at 0.0185 s sr^{-1} in the following three repeated measurements of the same setup (Fig. 7). This indicated that the glassy carbon had a high stability and the calibration procedure used here was repeatable for the same setup.

3.2.2. Reliability of the calibration between different setups. The reliability of the calibration procedure between different setups was tested by changing the experimental conditions with various J_{in} and L. Table 3 shows SF measured under different conditions using glass carbon as standard. According to equation (9), one can deduce that SF $\propto 1/(J_{in}\Delta\Omega)$, considering that $\eta(\lambda)$ remains unchanged as the energy of incident X-ray photons was kept at 10 keV here in all measurements. Centered on an arbitrary scattering direction, $\Delta\Omega$ can be written as

$$\Delta\Omega = \Delta S/R^2 = \Delta S/(L^2 + r^2), \qquad (17)$$

where ΔS is a single-pixel area on the detector, R is the distance between the sample and the pixel and r is the distance from the pixel to the center of the direct beam (Fig. 2). Here

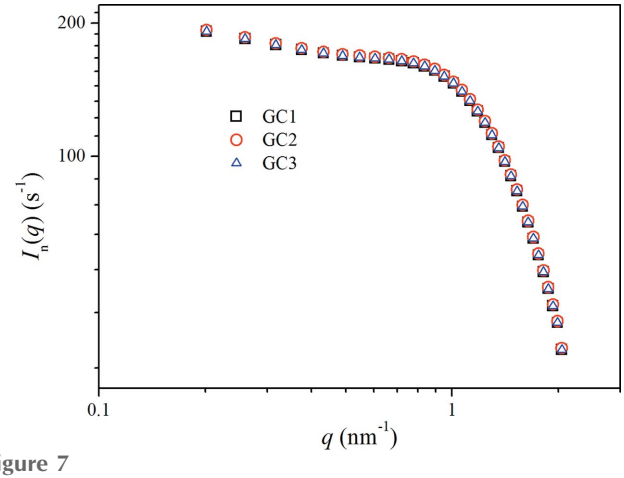

Figure 7
Repeated measurements of glass carbon scattering. GC1, GC2 and GC3 were the normalized intensity of the same setup, in which GC1 was that used in Fig. 6.

Table 3
SF at different setups on beamline BL16B1 of SSRF.

L (m)	J_{in} (10^{10} s^{-1})	L^2/J_{in} (10^{-10} m^2 s)	SF (s sr^{-1})
1.794	13.21	0.2436	0.0051
1.800	11.50	0.2817	0.0075
1.858	13.86	0.2491	0.0055
1.860	13.50	0.2563	0.0068
1.925	4.19	0.8844	0.0176
1.956	4.25	0.9002	0.0185
4.986	0.80	31.0752	0.7573
5.173	1.48	18.0810	0.4650

the geometric distortion between the plane detector surface and the X-ray propagation spherical surface is ignored considering the scattering angle 2θ is very small (less than 10°). Furthermore, as $r \ll L$, $\Delta\Omega$ can be rewritten as

$$\Delta\Omega \cong \Delta S/L^2. \qquad (18)$$

As a result it can be deduced that SF $\propto L^2/J_{in}$. Fig. 8 shows a good linear fit between the measured SF and the setup condition L^2/J_{in} (Table 3). This means that the calibration results were in line with the theoretical expectations and the calibration procedure was also reliable for different setups. For any SAXS equipment, as a rule of thumb, a prophetic SF calculating line can be determined using this method for the condition with constant incident photon energy that is frequently used. In particular, for the condition of 10 keV photon energy at BL16B1 at SSRF, the SF predicting line is

$$\mathrm{SF} = 2.471 \times 10^{-2}(L^2/J_{in}) - 1.123 \times 10^{-4}, \qquad (19)$$

where L is in m and J_{in} is in 10^{10} s^{-1}.

3.2.3. Calibration using pure water as second standard. Fig. 9 shows the measured scattering profile of pure water. It can be seen that the scattering of pure water is almost a horizontal line of small counts in the detected q range except for an increasing fluctuation close to q = 0. As pure water is a very weak scatterer, extending the exposure time can theoretically reduce the statistical error caused by noise fluctuations and relatively lower the effect of background scattering. Fig. 10 shows the 1D scattering intensity distribution of

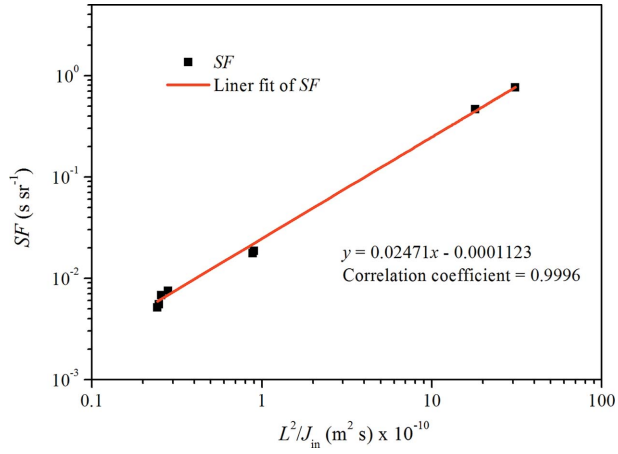

Figure 8
SF under various conditions and its linear fit *versus* L^2/J_{in}.

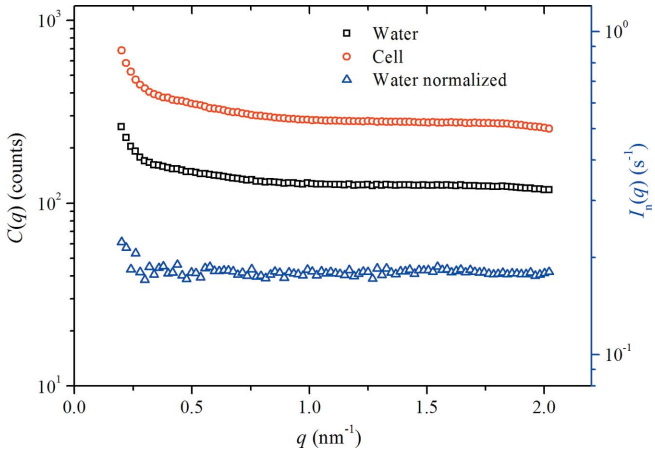

Figure 9
Scattering profile of pure water: raw intensity and normalization. The exposure time is 600 s for both the water and the cell.

water for the same setup in cases where the exposure time was 100, 300 and 600 s. The data divergence with longer exposure time was clearly reduced compared with that with shorter exposure time. This suggested that extending the exposure time of pure water as standard in the calibration procedure can improve the data quality and lower the potential statistical error. The subsequent measurements associated with water in the calibration were carried out with an exposure time of 600 s in order to insure more accuracy. However, the exposure time can be reduced accordingly when a beam of higher incident flux is used and a faster measurement can be performed.

By making a linear fit of $I_{\rm n,water}(q)/I_{\rm water}$ and comparing the intercept value with the theoretical $I_{\rm abs,water}(0)$ [equations (10)], SF can be obtained as 0.0193 s sr^{-1} (Fig. 11). Three repeated measurements were carried out and SF for the same setup was 0.0193, 0.0193 and 0.0190 s sr^{-1}, with an average value of 0.0192 s sr^{-1}. The maximum relative error was only 1.6% among these data, which suggested that pure water also has a very high stability as a calibration standard. Compared

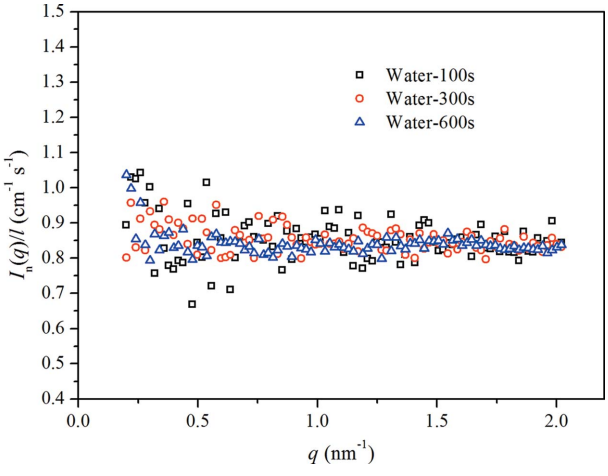

Figure 10
Scattering profile of pure water measured with different exposure times: water-100s, water-300s and water-600s were measured with exposure times of 100, 300, and 600 s, respectively.

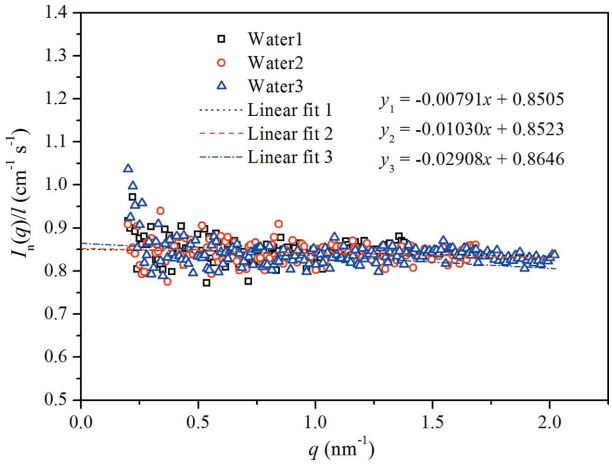

Figure 11
Scattering profiles of pure water and their linear fits. The measurements were repeated using the same setup three times and the calculated SF was 0.0193, 0.0193 and 0.0190 s sr^{-1}, respectively, with an average value of 0.0192 s sr^{-1}.

with the calibration results using glassy carbon as standard with the same setup, the mean value of SF obtained using pure water was approximately 3.8% larger. This indicates that, within an acceptable error range of less than 5%, water can be independently used as an effective secondary standard to calibrate the absolute scattering intensity.

4. Beamline performance on protein MW determination

4.1. Principle for protein MW determination using SAXS

Theoretically, the scattering length is the intrinsic scattering strength of a material to X-rays, and $I(q)$ is also described as the Fourier transform of the local scattering length density distribution (Glatter & Kratky, 1982). The scattering probability is derived from the difference in scattering length density between scattering inhomogeneities and the surrounding medium (Zhang *et al.*, 2009). For a dilute solution of monodisperse homogeneous solute particles, the scattering intensity difference between the solution and the solvent $\Delta I(q)$ is given by (Glatter & Kratky, 1982; Narayanan, 2008)

$$\Delta I(q) = N_{\rm p} V_{\rm p}^2 (\Delta\rho)^2 P(q), \qquad (20)$$

and the absolute scattering intensity difference is

$$\Delta I_{\rm abs}(q) = \frac{N_{\rm p} V_{\rm p}^2}{V} (\Delta\rho)^2 P(q) = c \frac{M}{N_{\rm A}} (\Delta\rho v)^2 P(q), \qquad (21)$$

where $N_{\rm p}$ is the total number of solute particles in the illuminated sample volume V, $V_{\rm p}$ (cm^3) is the volume of a single solute particle, c (g cm^{-3}) is the solute concentration, M (g mol^{-1}) is the molecular weight of the solute, $N_{\rm A}$ (6.02×10^{23} mol^{-1}) is Avogadro's constant, v (cm^3 g^{-1}) is the solute partial specific volume, $P(q)$ is the normalized form factor and $\Delta\rho$ (cm^{-2}) is the excess scattering length density between the solute and the solvent and can be calculate as follows (Mylonas & Svergun, 2007),

$$\Delta\rho = (n_{\rm solute} - n_{\rm solvent})\, r_{\rm e}, \quad (22)$$

where $n_{\rm solute}$ ($\rm cm^{-3}$) and $n_{\rm solvent}$ ($\rm cm^{-3}$) are the electron number density of solute and solvent, respectively, and $r_{\rm e}$ (2.82×10^{-13} cm) is the classical electron radius. The recommended value of $n_{\rm solute}$ and ν for proteins is 4.337×10^{23} $\rm cm^{-3}$ and 0.7425 $\rm cm^3\ g^{-1}$, respectively (Mylonas & Svergun, 2007). For dilute protein solution using water as solvent, $n_{\rm solvent}$ = 3.344×10^{23} $\rm cm^{-3}$ and $\Delta\rho$ is 2.800×10^{10} $\rm cm^{-2}$.

$\Delta I_{\rm abs}(q)$ can be acquired by measuring the scattering of solution and solvent separately, which afterwards are calibrated onto the absolute scale as

$$\Delta I_{\rm abs}(q) = {\rm SF}\left[I_{\rm n,solution}(q)/l_{\rm solution} - I_{\rm n,solvent}(q)/l_{\rm solvent}\right]. \quad (23)$$

Actually one can prepare the solution and solvent with the same thickness, *i.e.* $l_{\rm solution} = l_{\rm solvent} = l$, in the operations and $\Delta I_{\rm abs}(q)$ will be

$$\begin{aligned}\Delta I_{\rm abs}(q) &= {\rm SF}\,[I_{\rm n,solution}(q) - I_{\rm n,solvent}(q)]/l \\ &= {\rm SF}\,\Delta I_{\rm n}(q)/l. \end{aligned} \quad (24)$$

To achieve this, for example, one can use the same holder (such as a capillary or a cell) for both solution and solvent scattering detection on the condition that the solvent is used first and can be washed out. This will be convenient for data processing and avoid potential negative values for weakly scattering samples.

In the limit $q \rightarrow 0$, $P(0) = 1$, so that the molecular weight of the solute can be expressed as (Orthaber *et al.*, 2000; Jacques *et al.*, 2012)

$$M = \frac{N_{\rm A}\Delta I_{\rm abs}(0)}{c(\Delta\rho\nu)^2}. \quad (25)$$

In practical experiments, $\Delta I_{\rm abs}(0)$ cannot be measured directly; instead it can be obtained by making a Guinier approximation of $\Delta I_{\rm abs}(q)$ near $q = 0$ (Glatter & Kratky, 1982; Svergun & Koch, 2003; Putnam *et al.*, 2007; Hammouda, 2010; Schnablegger, 2011), which is

$$\Delta I_{\rm abs}(q) \cong \Delta I_{\rm abs}(0) \exp\left(-\frac{1}{3}q^2R_{\rm g}^2\right) \quad (26)$$

and

$$\ln \Delta I_{\rm abs}(q) \cong -\frac{1}{3}q^2R_{\rm g}^2 + \ln \Delta I_{\rm abs}(0), \quad (27)$$

where $R_{\rm g}$ is the gyration radius. A fitting of the linear segment near $q = 0$ in the Guinier plot $[\ln \Delta I_{\rm abs}(q) - q^2]$ enables one to extract the extrapolated intercept as $\ln \Delta I_{\rm abs}(0)$. This linear segment, called the Guinier region (Guinier & Fournet, 1955; Kostorz, 1979), is a very limited range in the low q region. In principle, the Guinier approximation is valid for a range not exceeding $q = 1.3/R_{\rm g}$ for globular particles, and for more asymmetric particles this limit approaches values around 1.0 and as small as 0.8 (Jacques *et al.*, 2012; Svergun & Koch, 2003). However, it is common in biological SAXS to extend this range up to $1.3/R_{\rm g}$, so that a sufficient number of data points are available for the estimation of $\Delta I_{\rm abs}(0)$ and $R_{\rm g}$. Practice shows that $1.3/R_{\rm g}$ is a safe estimate for the upper limit, which does not introduce systematic deviations from linearity (Mertens & Svergun, 2010). In practice, the Guinier fitting must be performed iteratively or interactively, since new estimates of $R_{\rm g}$ can alter the q range and $I_{\rm abs}(0)$ (Putnam *et al.*, 2007). It is important to determine M at several concentrations of the protein. Improper background subtraction, sample polydispersity or contamination, particle aggregation and interparticle interference caused by charge repulsion will result in deviations from linearity. In particular, aggregation will cause systematic upward curvature as q becomes smaller while repulsion will cause systematic downward curvature with decreasing q in the low q region (Jacques *et al.*, 2012). A fast determination M of multiple concentrations will give instant guidance in experimental operation and sample preparation.

4.2. Performance on molecular weight determination

Lysozyme (LYS), bovine serum albumin (BSA) and albumin from chicken egg-white (ALB, a special ovalbumin) were purchased from Sigma-Aldrich and used as protein samples. The known molecular weights of these proteins are 14.3, 66.0 and 45.0 kDa, respectively (Mylonas & Svergun, 2007). Solutions of five concentrations, 2, 4, 6, 8 and 10 mg $\rm ml^{-1}$, were prepared for each protein. Pure water with resistivity of 18 MΩ $\rm cm^{-1}$ was used as solvent to formulate the protein solution. Each solution was centrifugated for 10 min at a speed of 14000 rev $\rm min^{-1}$ before the scattering measurement. Three cells with mica windows of 20 µm thickness were used as the solution holders for the water and protein. The thickness of the cells was 1.924, 1.934 and 2.137 mm, according to calculations using the measured transmission coefficients of pure water. The transformation from 2D scattering graph to 1D scattering profile was carried out by circular averaging using the software *FIT2D*.

2D scattering of each liquid (solvent or solution) sample was quickly detected using a quite short exposure time of 100 s. The solvent and solution for the same protein were prepared with the same thickness. The SF of the setup was determined to be 0.0193 using pure water as the standard. Fig. 12 shows the 1D scattering profiles of solution, solvent and their difference in normalized scale. The scattering difference was calibrated onto the absolute scale (Fig. 13) before the Guinier fitting. The iteratively fitted upper q limits for BSA, LYS and ALB were 0.40, 0.80 and 0.45 $\rm nm^{-1}$, respectively. As an example, Fig. 13 shows the scattering intensity of BSA and Fig. 14 shows the corresponding Guinier plot. Decreases in intensity at very small q with increasing protein concentration of 6–10 mg $\rm ml^{-1}$ indicated the presence of increasing interparticle interference owing to charge repulsion. A similar phenomenon was found in LYS solutions at concentrations greater than 2 mg $\rm ml^{-1}$ and in ALB solutions at concentration greater than 2 mg $\rm ml^{-1}$. Repulsion can be dealt with by dilution or increasing ionic strength (Putnam *et al.*, 2007). It is necessary to adjust the solvent composition or pH to reduce this effect in defining accurate macromolecular structures. However, as a pre-diagnosis, it is more straight-

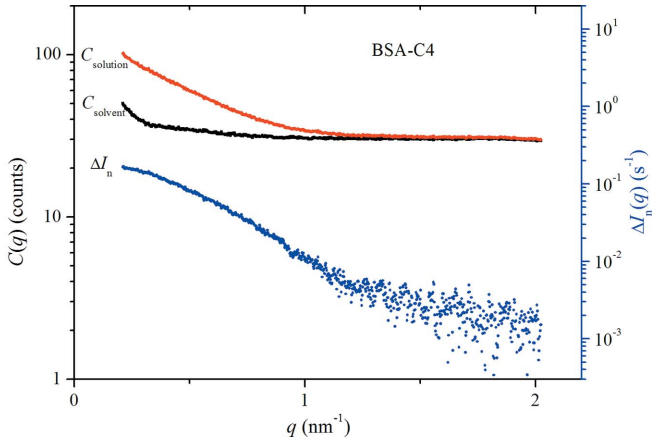

Figure 12
Profile of the scattering difference between BSA solution with a concentration of 4 mg ml^{-1} (BSA-C4) and the water solvent.

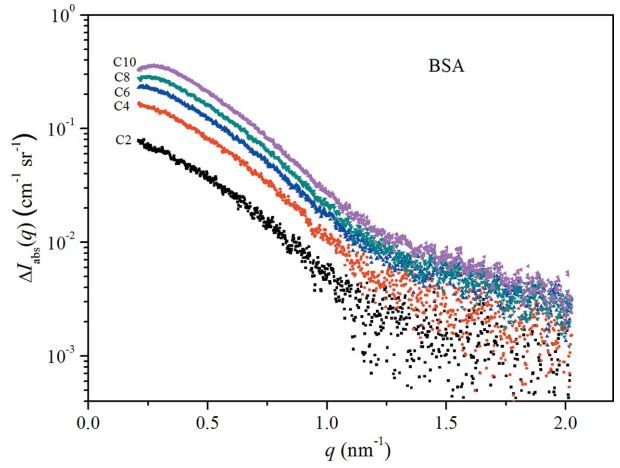

Figure 13
Absolute scattering intensity of BSA in solution with various concentrations. SF is 0.0193 and C2, C4, C6, C8 and C10 have concentrations of 2, 4, 6, 8 and 10 mg ml^{-1}, respectively. Decreases in intensity at very small q in samples C6, C8 and C10 indicate the presence of increasing interparticle interference owing to charge repulsion.

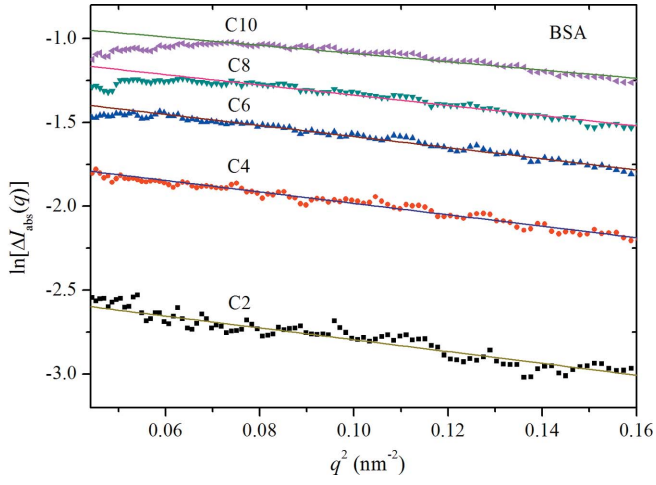

Figure 14
Guinier plots and fitting for BSA scattering in solutions of various concentrations. The more clearly displayed downturns (compared with Fig. 13) at low q for C6–C10 give indications of interparticle repulsion with increasing protein concentration.

Table 4
Fitted parameters and calculated M of BSA (kDa).

c (g ml^{-1})	R_g (nm)	$1.3/R_g$ (nm^{-1})	$I_{abs}(0)/c$ (cm^2 g^{-1})	M (kDa)	Δ (%)†
0.002	3.25 ± 0.07	0.40	43.5 ± 0.7	60.5 ± 1.0	−8.3
0.004	3.20 ± 0.04	0.41	48.4 ± 0.4	67.5 ± 0.6	2.2
0.006	3.15 ± 0.03	0.41	47.6 ± 0.3	66.3 ± 0.4	0.4
0.008	3.03 ± 0.03	0.43	44.6 ± 0.3	62.1 ± 0.4	−5.9
0.010	2.72 ± 0.04	0.48	43.1 ± 0.3	60.0 ± 0.5	−9.0

† Compared with the known value of 66.0 kDa (Mylonas & Svergun, 2007).

Table 5
Fitted parameters and calculated M of LYS.

c (g ml^{-1})	R_g (nm)	$1.3/R_g$ (nm^{-1})	$I_{abs}(0)/c$ (cm^2 g^{-1})	M (kDa)	Δ (%)†
0.002	1.33 ± 0.06	0.98	10.8 ± 0.2	15.0 ± 0.3	5.2
0.004	1.56 ± 0.07	0.83	9.6 ± 0.3	13.3 ± 0.5	−6.9
0.006	1.60 ± 0.02	0.81	10.4 ± 0.2	14.6 ± 0.1	1.8
0.008	1.46 ± 0.02	0.89	10.2 ± 0.2	14.2 ± 0.1	−0.5
0.010	1.47 ± 0.02	0.88	9.8 ± 0.2	13.6 ± 0.1	−4.9

† Compared with the known value of 14.3 kDa (Mylonas & Svergun, 2007).

Table 6
Fitted parameters and calculated M of ALB.

c (g ml^{-1})	R_g (nm)	$1.3/R_g$ (nm^{-1})	$I_{abs}(0)/c$ (cm^2 g^{-1})	M (kDa)	Δ (%)†
0.002	2.81 ± 0.13	0.46	34.1 ± 1.1	47.4 ± 1.5	5.4
0.004	2.91 ± 0.08	0.45	35.1 ± 0.7	48.9 ± 0.9	8.8
0.006	2.89 ± 0.06	0.45	30.2 ± 0.4	42.1 ± 0.6	−6.5
0.008	2.87 ± 0.03	0.45	29.6 ± 0.2	41.2 ± 0.3	−8.4
0.010	2.77 ± 0.04	0.47	30.2 ± 0.3	42.1 ± 0.4	−6.4

† Compared with the known value of 45.0 kDa (Mylonas & Svergun, 2007).

forward to prepare solutions of multiple concentrations to find the adequate diluted ones before adjusting. As shown in Figs. 13 and 14, the downturn in the low q region is vanishing in the more dilute solutions with protein concentration of 2–4 mg ml^{-1}.

Tables 4, 5 and 6 list the fitted parameters in the Guinier approximation. An overall decrease in fitted R_g also provided evidence that samples of higher concentration were undergoing charge repulsion which should be eliminated as much as possible in more accurate structural characterization. The measured MWs of high concentrations ($\geq$8 mg ml^{-1}) were also being underestimated due to repulsive interactions as shown in Tables 3–5. However, compared with known values, the measured MW of protein here in each single concentration had a deviation within 10% (Tables 3–5), which is also the best attainable accuracy in recent studies using SAXS to measure protein molecular weight (Fischer *et al.*, 2010; Mylonas & Svergun, 2007; Jacques *et al.*, 2012). This consistency revealed that the repulsion was not fatal for the Guinier approximation at concentrations of 2–10 mg ml^{-1} for the proteins used here. It provided major confidence that the sample contained monodisperse particles of the expected composition. It also suggested that the absolute intensity calibration using water as standard reference and the molecular weight determination

were quite reliable with considerable accuracy. The method demonstrated here provided a rapid practicable *in situ* way to measure the protein MW directly in minutes without measuring standard protein materials. It enables a quick instant check or pre-diagnosis of the sample preparation and experiment operation to improve the data quality during the SAXS performance, especially during the queuing experiments of limited allocated beam time using synchrotron X-ray sources.

5. Conclusion and perspectives

Beamline BL16B1 at SSRF was designed and constructed for SAXS-related studies in 2009 and is open to users with several methodologies and a series of supporting equipment. The scattering intensity in SAXS was distinguishingly re-stated in this work as $C(q)$, $I(q)$ and $I_{abs}(q)$ according to the extent of data processing and $I_{abs}(q)$ was suggested to be a unified presentation of SAXS data. Theory together with practical procedures for calibration of $I_{abs}(q)$ was established based on the SAXS configuration of this beamline, using glass carbon and water as primary standard and secondary standard, respectively. The calibration performance was tested repeatedly and showed a high reliability in different setups. A prophetic line can be determined to estimate SF in various setups using this method for any specific SAXS setups. The calibration can be effectively completed in minutes and used for fast protein MW determination. Results showed good accuracy with a deviation within 10% compared with known values and revealed the presence of charge repulsion caused by a flaw in sample preparation. This provided confidence in the beamline performance both on the absolute intensity calibration and protein MW determination. Fast MW measurement in minutes at the beamline can be used to make an instant check for the sample preparation and experiment operation to improve the data quality for in-depth analysis during the SAXS performance, especially during the queuing experiments of limited allocated beam time using synchrotron X-ray sources.

Acknowledgements

The authors acknowledge financial support from the National Natural Science Foundation of China (No. 11305242, 11305249, U1432115). We would like to thank Jan IIavsky at APS, Argonne National Laboratory, for providing the glass carbon sample and its data.

References

Cyranoski, D. (2009). *Nature (London)*, **459**, 16–17.
Fan, L., Degen, M., Bendle, S., Grupido, N. & Ilavsky, J. (2010). *J. Phys. Conf. Ser.* **247**, 012005.
Fischer, H., de Oliveira Neto, M., Napolitano, H. B., Polikarpov, I. & Craievich, A. F. (2010). *J. Appl. Cryst.* **43**, 101–109.
Glatter, O. & Kratky, O. (1982). *Small-Angle X-ray Scattering.* London: Academic Press.
Guinier, A. & Fournet, G. (1955). *Small-Angle Scattering of X-rays.* New York: John Wiley and Sons.
Hammouda, B. (2010). *J. Appl. Cryst.* **43**, 716–719.
Hu, Z., Mi, Q. R., Zhen, L. F. & Li, Z. (2014). *Nucl. Sci. Tech.* **25**, 020103.
Huang, Y. F., Xu, J. Z., Xu, J. Y., Zhang, Z., Hsiao, B. S., Xu, L. & Li, Z. (2014). *J. Mater. Chem. B*, **2**, 971–980.
Ilavsky, J. & Jemian, P. R. (2009). *J. Appl. Cryst.* **42**, 347–353.
Jacques, D. A., Guss, J. M., Svergun, D. I. & Trewhella, J. (2012). *Acta Cryst.* D**68**, 620–626.
Kostorz, G. (1979). *Small Angle Scattering and its Application to Material Science* in *Neutron Scattering*, Vol. 15, pp. 227–289. New York: Academic Press.
Li, F. G., Zhang, J., Dai, Y. B., Bian, F. G., Han, Y. F. & Sun, B. D. (2014). *Mater. Chem. Phys.* **143**, 471–475.
Li, T., Senesi, A. J. & Lee, B. (2016). *Chem. Rev.* **116**, 11128–11180.
Lide, D. R. (2005). *CRC Handbook of Chemistry and Physics* (Internet version). Boca Raton: CRC Press.
Liu, G. M., Zheng, L. C., Zhang, X. Q., Li, C. C. & Wang, D. J. (2014). *Macromolecules*, **47**, 7533–7539.
Mertens, H. D. T. & Svergun, D. I. (2010). *J. Struct. Biol.* **172**, 128–141.
Mylonas, E. & Svergun, D. I. (2007). *J. Appl. Cryst.* **40**, s245–s249.
Narayanan, T. (2008). *Small-Angle X-ray Scattering in Soft Matter Characterization*, edited by R. Borsali and R. Pecora, Vol. 45, pp. 899–952. Dordrecht: Springer Netherlands.
Orthaber, D., Bergmann, A. & Glatter, O. (2000). *J. Appl. Cryst.* **33**, 218–225.
Pauw, B. R. (2013). *J. Phys. Condens. Matter*, **25**, 383201.
Pleštil, J., Pospíšil, H., Ostanevich, Yu. M. & Degovics, G. (1991). *J. Appl. Cryst.* **24**, 659–664.
Putnam, C. D., Hammel, M., Hura, G. L. & Tainer, J. A. (2007). *Q. Rev. Biophys.* **40**, 191–285.
Roe, R. J. (2000). *Methods of X-ray and Neutron Scattering in Polymer Science.* New York: Oxford University Press.
Schnablegger, H. (2011). *The SAXS Guide: Getting Acquainted with the Principles.* Austria: Anton Paar GmbH.
Svergun, D. I. & Koch, M. H. J. (2003). *Rep. Prog. Phys.* **66**, 1735–1782.
Tian, F., Li, X. H., Wang, Y. Z., Yang, C. M., Zhou, P., Lin, J. Y., Zeng, J. R., Hong, C. X., Hua, W. Q., Li, X. Y., Miao, X. R., Bian, F. G. & Wang, J. (2015). *Nucl. Sci. Tech.* **26**, 030101.
Weinberg, D. L. (1963). *Rev. Sci. Instrum.* **34**, 691–696.
Xu H. J. & Zhao Z. T. (2008). *Nucl. Sci. Tech.* **19**, 1–6.
Yang, C. M., Bian, F. G., Xiong, B. Q., Liu, D. M., Li, Y. W., Hua, W. Q. & Wang, J. (2016). *Chin. Phys. B*, **25**, 066101.
Zhang, F., Ilavsky, J., Long, G. G., Quintana, J. P. G., Allen, A. J. & Jemian, P. R. (2009). *Met. Mater. Trans. A*, **41**, 1151–1158.
Zhou, W. M., Meng, L. P., Lu, J., Wang, Z., Zhang, W. H., Huang, N. D., Chen, L. & Li, L. B. (2015). *Soft Matter*, **11**, 5044–5052.
Zhu, Y. P. (2008). *Small Angle X-ray scattering.* Beijing: Chemical Industry Press. (In Chinese.)